Research Article | Vol. 31, No. 8 / 10 Apr 2023 / Optics Express 12289
Optics EXPRESS

Versatile OSCAT time-domain THz spectrometer

LISA M. MOLTENI,[1,2] JACOPO MANZOLLI,[1] FEDERICO PIRZIO,[3] ANTONIANGELO AGNESI,[3] GIULIANO PICCINNO,[4] PAOLO LAPORTA,[1,2] AND GIANLUCA GALZERANO[2,5,*]

[1]*Dipartimento di Fisica, Politecnico di Milano, 20133 Milano, Italy*
[2]*Istituto di Fotonica e Nanotecnologie - Consiglio Nazionale delle Ricerche, 20133 Milano, Italy*
[3]*Dipartimento di Ingegneria Industriale e dell'Informazione, Università Pavia, Via Ferrata 5, 27100 Pavia, Italy*
[4]*Bright Solutions SRL, Via degli Artigiani 27, 27010 Cura Carpignano (PV), Italy*
[5]*Istituto Nazionale di Fisica Nucleare, Sezione di Milano, via Celoria 16, 20133, Milan, Italy*
[*]*gianluca.galzerano@polimi.it*

Abstract: We report on a compact and versatile time-domain spectrometer operating in the THz spectral region from 0.2 to 2.5 THz based on ultrafast Yb:CALGO laser and photo-conductive antennas. The spectrometer operates with the optical sampling by cavity tuning (OSCAT) method based on laser repetition rate tuning, which allows at the same time the implementation of a delay-time modulation scheme. The whole characterization of the instrument is presented and compared to the classical THz time-domain spectroscopy implementation. THz spectroscopic measurements on a 520-μm thick GaAs wafer substrate together with water vapor absorption measurements are also reported to further validate the instrument capabilities.

1. Introduction

Time-domain spectroscopy (TDS) in the terahertz (THz) region is becoming a fundamental and useful tool in a large variety of applications in the fields of nondestructive testing [1,2], imaging [3–5] and microscopy [6–8], security [9,10], material science [11,12], biomedicine [13,14], analytical and molecular spectroscopy [15,16], and communications [17,18]. Conventional THz-TDS systems use a femtosecond laser and electro-optical or photoconductive sampling to reconstruct the THz electromagnetic field using mechanical delay line for tuning the time delay between the received THz pulse and the sampling optical pulse [19,20]. Depending on the spectral resolution requirements of the THz-TDS, the scanning time, in general, has to be tuned in the range from 10 to 100 ps or even larger time by scanning the mechanical delay line up to few centimeters. This mechanical excursion requires a measurement time for a single THz waveform from several tenths of seconds to several seconds. These acquisition times can limit the use of the classical THz-TDS in all applications of real-time sensing and hyperspectral imaging that require a high acquisition speed of the THz spectra. For this reason, in recent years different experimental techniques have been investigated to increase the acquisition speed of the THz-TDS: using faster mechanical delay line (fast rotating delay line or galvanometer systems) [21,22], employing asynchronous optical sampling and dual comb techniques [23–25], and by laser cavity tuning [26,27] methods.

In this paper, we present a versatile implementation of a THz-TDS based on a low-energy laser source emitting 70-fs pulse-train at 1 μm with tunable pulse repetition frequency (more than 1% of its average value) and photo-conductive antennas (PCAs) [28]. Fast delay-time tuning covering more than 100 ps with a rate of 10 scan/s is achieved by using the optical sampling by cavity tuning (OSCAT) method [26,29]. The OSCAT method relies on the use of a fixed delay line to combine pulse pair on the receiver PCA with different order (many pulse repetition periods) and change their temporal superposition by acting on the laser pulse repetition frequency.

#482396 https://doi.org/10.1364/OE.482396
Journal © 2023 Received 1 Dec 2022; revised 27 Feb 2023; accepted 28 Feb 2023; published 29 Mar 2023

Optics EXPRESS

Indeed, indicating with M the order difference between the superimposed pulses, the temporal delay between the pulses changes on the basis of the following equation $\Delta\tau = M\Delta f_r/[f_r(f_r + \Delta f_r)]$, where f_r is the pulse repetition frequency and Δf_r is its change. The spectrometer also allows the effective implementation of the delay time modulation (DTM) technique to retrieve the first derivative in time of the THz field [30], which turns out to be extremely interesting for sensing methods related to the phase variations of the THz field. The complete characterization of the developed THz-TDS is presented together with the comparison of the OSCAT and DTM methods with respect to the classical implementation of THz TDS. The fast scanning performance is also characterized, obtaining single scan OSCAT measurements in 80 ms acquisition time and signal-to-noise ratio (SNR) of 56 (35 dB) for 1 ms lock-in integration time. Finally, the measurements of the refractive index and absorption coefficient of a GaAs plate together with the absorption spectrum of water vapor are reported.

2. Experimental setup

Figure 1 shows the realized THz TDS setup. The ultrafast source is a passive mode-locked Yb:$CaGdAlO_4$ (Yb:CALGO) laser operating in the spectral region at around 1045 nm emitting hyperbolic secant pulses with 74 fs duration (see Fig. 2), optical bandwidth of ~21 nm (full width at half maximum, FWHM), 60 mW average power, and a repetition frequency of 160 MHz. The linear cavity configuration and additional details on the laser source are reported in [31]. The laser output coupler is mounted on a voice coil linear stage (PI mag V-528) that can change the cavity length by ±10 mm around its central value of 0.937 m with a maximum speed of 250 mm/s, corresponding to a pulse repetition frequency variation of ±1.5 MHz at the maximum rate of 30 kHz/ms, as shown in Fig. 3(a) where the pulse repetition frequency (measured using an electronic frequency counter) is reported as a function of time. Periodic linear modulation of the pulse repetition rate can be also achieved with a maximum scanning rate of 10 scan/s, as shown in Fig. 3(b). Fine tuning of the pulse repetition frequency is obtained by acting on a piezoelectric ceramic glued on the intracavity semiconductor saturable absorption mirror (SESAM) with a dynamic of ~ 1.7 kHz (for 150 V) and a maximum high-signal bandwidth of 2 kHz. The PZT actuator is used either to stabilize the repetition frequency against a RF synthesizer or to apply a fast modulation to the pulse repetition rate. Figure 3(c) shows the RF spectrum at around 160 MHz when a sinusoidal voltage with peak-to-peak amplitude of 75 V and 1 kHz frequency is applied to the PZT, corresponding to a frequency modulation depth of 427 Hz.

For the generation and detection of the THz radiation the Yb:CALGO pulse train is splitted by a 50% beam splitter (BS) into two distinct arms that are then sent to fiber-coupled PCAs realized with a low temperature growth InGaAs photocondutive susbstrate (carrier recovery time 300 fs) on a GaAs wafer substrate (BATOP optoelectronics). The emitter PCA is a parallel-line (electric dipole) antenna with a length of 40 μm, a gap distance of 5 μm, and a width of 10 μm. The maximum voltage across the antenna is 20 V. The emitter PCA is supplied with a square wave signal with a peak-to-peak voltage excursion of ±20 V and a frequency ranging from 1 to 10 kHz. Alternatively, a DC bias of 20 V can be used when the delay time modulation scheme is adopted. The receiving antenna is a Bowtie antenna with a length of 100 μm, a gap of 5 μm, and a width of 10 μm. The maximum incident optical power on each PCA is ~15 mW. Both PCAs are fiber-coupled with 1-m long polarization maintaining (PM) fiber and equipped with hyperhemispherical silicon substrate lenses to either collimate (emitter) or focalize (receiver) the THz radiation. A fixed delay line, consisting of a 20-m long single-mode PM fiber, is inserted in the TDS receiver arm to implement OSCAT [26,29] and DTM [30] methods. Each arm of the TDS contains proper transmission grating pair (800 grooves/mm operating at an incident angle of 23°) to compensate the group delay dispersion introduced by the optical fibers coupled to the PCAs. The THz pulse is detected by a lock-in amplifier connected to the receiver PCA, whose output signal is recorded by an analog-to-digital acquisition board (24 bit at 1 MS/s) together

Optics EXPRESS

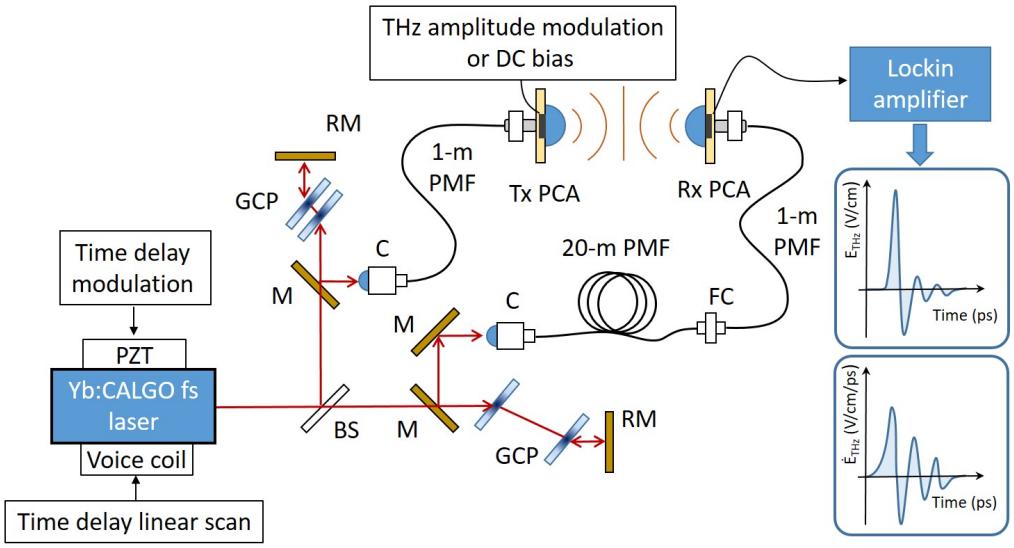

Fig. 1. Experimental layout of the THz TDS. BS: beam splitter; C: fiber collimator; FC: fiber connector; GCP: grating compressor pair; M: mirror; PCA: photoconductive antenna; PMF: polarization maintaining fiber; PZT: piezoelectric; RM: roof mirror.

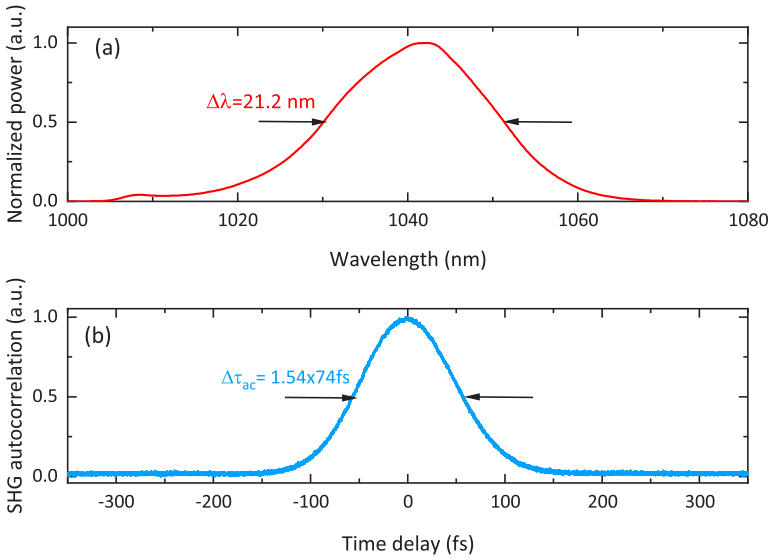

Fig. 2. (a) Pulse optical spectrum and (b) intensity autocorrelation of the Yb:CALGO mode-locked laser (average power 60 mW).

with the frequency counter for the time delay axis real-time calibration. The scanning of the delay time between THz and optical pulses at the receiver PCA is performed through the linear tuning of the pulse repetition frequency, acting on the Yb:CALGO voice coil linear stage. In the OSCAT method, THz and optical pulses at the receiver PCA superimpose with an optical path difference of about 30 m (assuming a refractive index of 1.5 for the 20-m long optical fiber), corresponding to a different pulse order of $M = 15$. This pulse order difference allows a straightforward calculation of the time-delay tuning coefficient with respect to pulse repetition

Optics EXPRESS

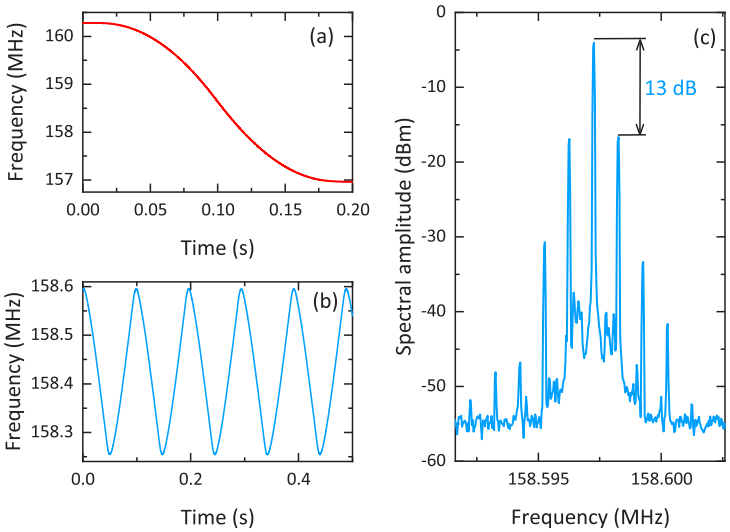

Fig. 3. (a) Single scan of the pulse repetition frequency using voice coil stage covering the full dynamic of ~3.4 MHz in 0.2 s (maximum speed of ~ 30 kHz/ms). (b) Periodic linear scan of the pulse repetition frequency with an amplitude of 350 kHz at the rate of 10 scan/s (corresponding to a linear scan speed of 6 kHz/ms). (c) RF spectrum at around the pulse repetition frequency when at the PZT actuator is applied a sinusoidal voltage with a peak-to-peak amplitude of 75 V at a modulation frequency of 1 kHz. From the side-bands intensity a frequency modulation depth of 427 Hz is measured.

frequency variation $\Delta\tau/\Delta f_r = M/f_r^2 = 0.63$ ps/kHz. Acting on the linear voice coil actuator, a maximum scanning time delay of ±0.9 ns can be obtained whereas using the PZT actuator with a modulation depth of 427 Hz (as shown in Fig. 3(b)) a sinusoidal modulation of the time delay up to ±270 fs is achieved.

3. THz-TDS characterization

The THz spectrometer can be operated in three different measurement schemes: i) the OSCAT method, scanning the pulse repetition frequency and therefore the delay time between THz and optical pulses on the receiver PCA by means of the linear voice coil stage; ii) the classical TDS approach, removing the 20-m long fiber and scanning the position of the fiber-receiver collimator (C) mounted on an external linear stage); iii) the DTM method, acting on the PZT for the time delay sinusoidal modulation and on the voice coil for the linear pulse repetition frequency scan. In the first two implementations, the emitter PCA is modulated by a square-wave voltage with ±20 V and 5 kHz frequency, whereas in the third scheme the emitter is simply biased by a DC voltage of 20 V. In this last case, being the emitting PCA unmodulated a significant reduction of parasitic electrical induction between the two PCAs is obtained. Figure 4(a) shows the THz field recorded at the output of the lock-in amplifier (sensitivity 0.5 nA and integration time of 100 ms) in the case of OSCAT implementation together with that acquired with the classical TDS scheme. Time delay calibrations were performed using an electronic counter to measure the instantaneous pulse repetition frequency in the case of the OSCAT measurement whereas for the classical TDS scheme by using the absolute position of the external linear stage (absolute optical encoder). It is worth noting that the recorded OSCAT profile, acquired in 10 s (ten time faster than the TDS trace that was recorded by using a slow motorized linear stage), does not exhibit any significant broadening with respect to the TDS profile, indicating a negligible contribution of the laser

Optics EXPRESS

pulse-to-pulse time jitter in the selected measurement times [27]. This behavior is also confirmed by the spectra of the measured THz pulse profile reported in Fig. 4(b): the OSCAT spectrum does not present a significant spectral narrowing. Indeed, the measured timing-pulse jitter of the femtosecond Yb:CALGO laser is below 70 fs (pulse duration) for integration bandwidth from 10 MHz down to 10 kHz [31], indicating that this method can be used without significant degradation up to pulse orders of ~1000. In both configurations (OSCAT and classic TDS) the spectral coverage above the noise floor ranges from 0.25 to 2.5 THz with the central frequency located at 0.9 THz.

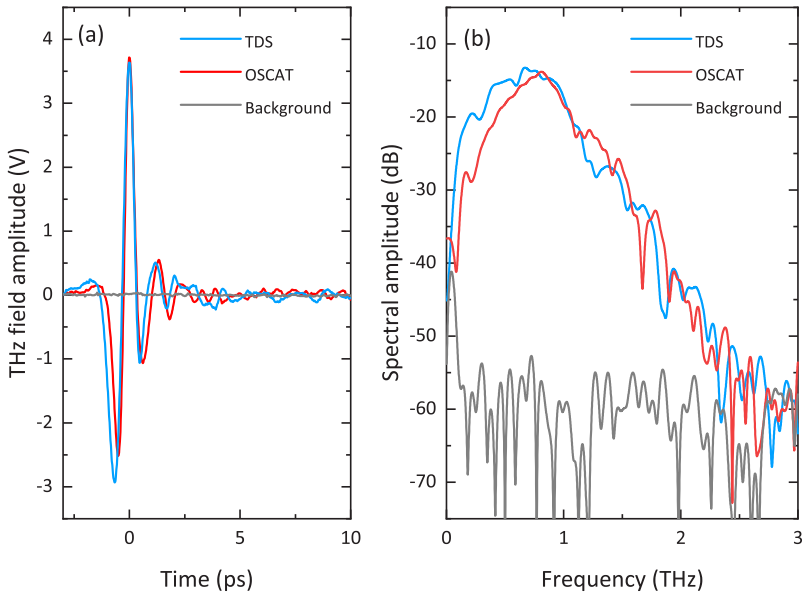

Fig. 4. Measured THz pulses (a) and corresponding spectra (b), for the OSCAT (red curves) and classical TDS (blue curves) implementations using the same experimental parameters: 10 mW optical power on each PCA; modulation frequency 5 kHz; Lock-in sensitivity 0.5 nA, 100 ms integration time.

To better investigate the spectral resolution of the implemented OSCAT method, Fig. 5(a) reports a longer temporal acquisition of the THz pulse as the measured with a lockin amplifier integration time of 100 ms. The emitted THz pulse passes over, 5 cm apart, a baker (10-cm in diameter) filled with liquid water at a temperature of ~90°C. In Fig. 5(a) the measured SNR with respect to the peak of the THz pulse is ~500, as computed using for the noise floor a root mean square value of 5 mV (see noise panel in Fig. 5(a)). Strong temporal oscillations can be observed even at delay times very far from the peak of the THz pulse (see H_2O absorptions panel in Fig. 5(a) showing the THz signal at 30-ps delay from the peak value). These oscillations are a clear evidence of the water vapor absorption rotational lines that interact with the THz radiation. A better evidence of the water absorption profile is shown in the THz spectrum reported in Fig. 5(b). Many water vapor absorption lines can be observed in the spectral range from 0.5 to 2.2 THz appearing as amplitude modulations of the THz spectrum. By using a rectangular window and a 100% zero-padding of the data reported in Fig. 5(a), a spectral resolution of 8.6 GHz is obtained. The linewidths, full width at half maximum, of the measured water vapor absorption lines are ranging from 19 to 25 GHz in a quite good agreement with the 16-GHz value computed using HITRAN database [32]. In addition, by comparing the measured spectrum with the HITRAN computed one, a frequency accuracy in the measurement of the water vapor line center frequencies better than 2.5 GHz (3 times lower than the frequency resolution), as

Optics EXPRESS

determined by the root-mean square value of the frequency differences between the measured and computed linecenter frequencies, is also demonstrated.

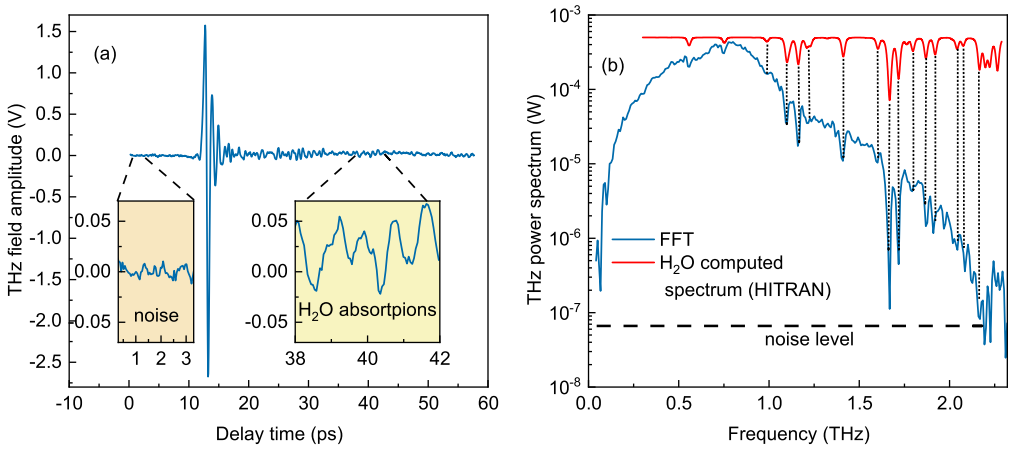

Fig. 5. Measured THz pulse (a) and corresponding spectrum (b), for the OSCAT spectrometer recorded with a locking integration time of 100 ms. The red curve reported in panel (b) is the water vapor absorption spectrum computed by HITRAN database [32]. A frequency resolution of 26 GHz is obtained using a rectangular window and 100% zero-padding.

Fast scanning acquisition performance of the OSCAT method is also characterized by applying to the laser voice coil a periodic ramp with a scanning delay-time of 10 ps and a rate of 4 Hz (limited by the minimum 1-ms integration time of the lock-in amplifier). Figures 6(a) and (b) show the pulse repetition frequency acquired by the electronic counter as a function of laboratory time and the OSCAT signal at the output of the lock-in amplifier as recorded by a 12-bit digital oscilloscope. It is worth noting that despite the short lock-in integration time of 1 ms a pretty good SNR of 35 (corresponding to 31 dB, as calculated from the FFT spectrum) is obtained for a single-scan acquisition time of 80 ms (corresponding to a delay time rate of 0.1 ps/ms). This SNR ratio can be further increased to 35 dB by filtering in real time the OSCAT trace by a fourth-order low-pass Butterworth digital filter (4-kHz cut-off frequency), which reduces the spurious second harmonic signal (10 kHz) at the lock-in amplifier output. Higher SNR can be obtained by averaging several sequential fast scanning traces. For example, Fig. 6(c) reports the OSCAT trace corresponding to 100 averages showing a SNR of 400 (52 dB), in close agreement with the $N^{1/2}$ law (where N is the number of averaged signals). Figure 6(d) shows the SNR as a function of the number of averages together with the $N^{1/2}$ fitting curve. At 1000 averages (corresponding to an acquisition time of 80 s) a slight deviation from the $N^{1/2}$ law appears due to a combination of THz intensity noise and time jitter fluctuations.

The DTM method has been also fully characterized in comparison to the OSCAT scheme. Figure 7(a) shows the lock-in output signal in the case of the DTM, first harmonic demodulation, compared to the THz pulse recorded in the OSCAT scheme, using the same experimental parameters apart the different modulation schemes (1 kHz modulation frequency with a delay time modulation of 270 fs). In Fig. 7(a) also the computed first derivative profile of the OSCAT signal is shown. It is worth noting that the first harmonic signal strongly resembles to the first derivative profile as highlighted by the residuals reported in Fig. 7(b), in agreement with the general behaviour of a low modulation index of the time-delay. Under the assumption of a small modulation index, the demodulated signal can be approximated by a Taylor-series expansion of the OSCAT profile. In the diagram reported in Fig. 7(b) is also shown the third derivative signal of the OSCAT profile indicating that for the implemented configuration of the DTM scheme the

Optics EXPRESS

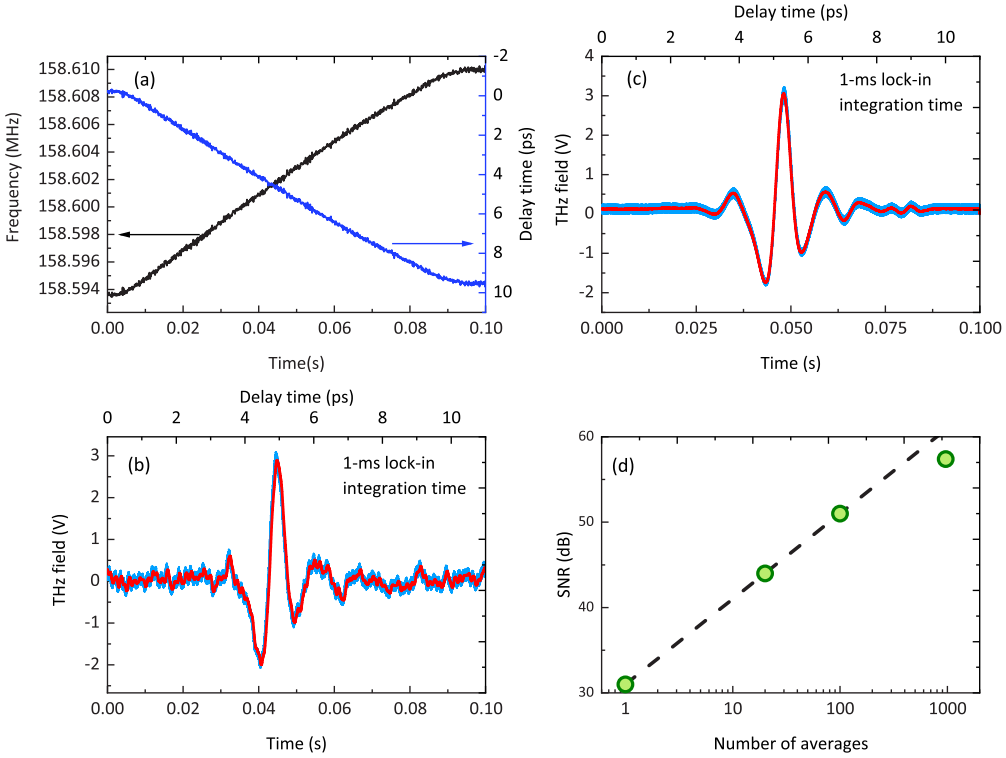

Fig. 6. (a) Pulse repetition frequency as a function of laboratory time measured by an electronic counter (100 μs gate time). (b) Fast scanning OSCAT time trace recorded by a 12-bit digital oscilloscope (1-ms lock-in integration time). (c) OSCAT signal corresponding to the average of 100 sequential scan traces. In both panel (b) and (c) the red curves represent the numerically filtered OSCAT trace by a fourth-order low-pass Butterworth filter (4-kHz cut-off frequency) to reduce the second harmonic spurious signal at the lock-in amplifier output. (d) SNR as a function of the number of average together with the $N^{1/2}$ law fitting curve.

first harmonic signal depends on the first term of the Taylor series of the OSCAT signal, being the third derivative term more than 10 time smaller than the first derivative contribution (small modulation of 270-fs with respect to the ~1 ps THz pulse width). The normalized amplitude spectra in a logarithmic scale of the DTM signal and of the OSCAT with in addition its first derivative profiles are shown in Fig. 7(c). Also in the Fourier frequency domain there is a good agreement between the spectra of the first harmonic demodulated signal and the first derivative one. From the comparison of the recorded time traces in Fig. 7(a), it can be seen that the signal-to-noise-ratio (SNR) is degraded in the DTM method with respect to the OSCAT signal by a factor of 5 (with the same 100-ms lock-in integration time), although the comparison is not related to the same quantity (OSCAT retrieves the THz electric field whereas DTM gives the first derivative of the THz electric field). The numerical integration of the first derivative signal can therefore be used to make a real comparison of the two methods in terms of SNR and detection sensitivity. Figure 7(d) shows the comparison of the OSCAT and the integrated DTM traces showing for the integrated signal a slightly better SNR with respect to the OSCAT trace.

Finally, to test the performance of the THz spectrometer, the measurement of refractive index and absorption of an intrinsic GaAs wafer with a thickness of 520 ± 5 μm has been performed. Figure 8 summarizes the results obtained by the OSCAT and DTM methods. Real and imaginary

Optics EXPRESS

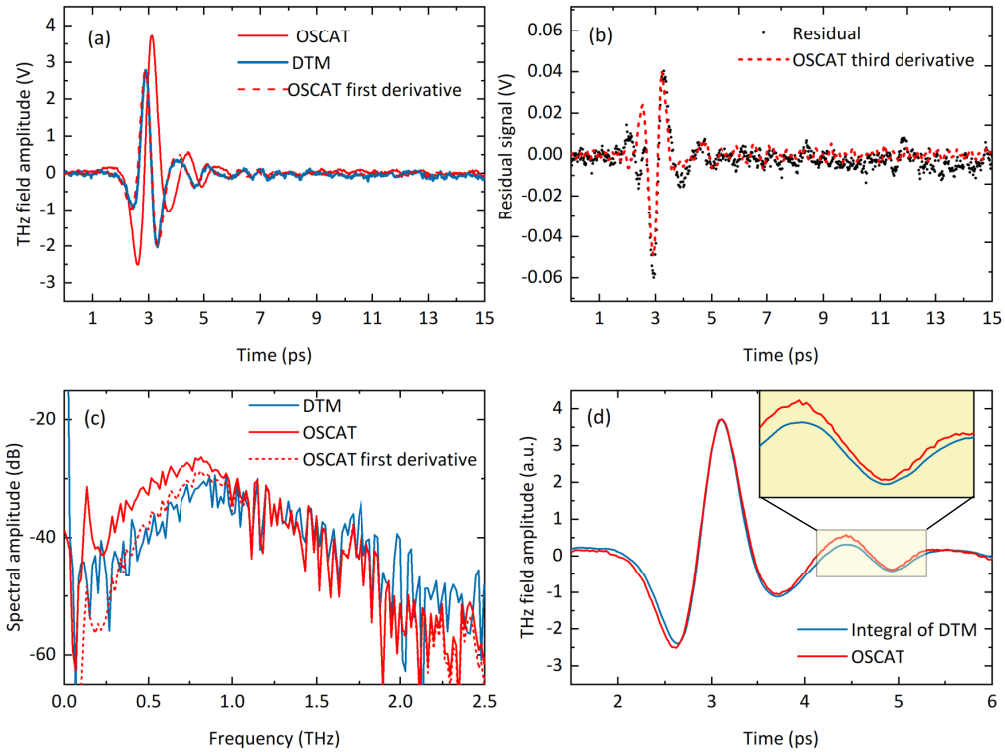

Fig. 7. (a) DTM signal, first harmonic demodulation, at the locking amplifier output (blue curve) together with the OSCAT profile (red curve) and its computed first derivative profile (dashed red curve). (b) Difference between the DTM signal and the computed first derivative together with the third derivative profile of the OSCAT signal (dotted red curve). (c) FFT spectra of the signals. (d) Integrated DTM (blue curve) together with the OSCAT profile (red curve) as a function of time. Inset: zoom of the traces to highlight the better SNR of the integrated profile with respect to the OSCAT one. In all diagrams the lock-in amplifier integration time is 100 ms.

parts of the complex refractive index are retrieved using conventional THz-TDS analysis for the OSCAT measurement taking into account also the etalon (multiple reflections) effect [19,20]. Indeed, Fig. 8(a) clearly shows the temporal replicas of the THz pulse with a time separation of 12.49 ps corresponding to the round trip time of the multiple reflections on the 520-μm thick GaAs plate ($t_{rt} = 2nt/c$, where n is the GaAs refractive index, t is GaAs thickness, and c is the vacuum speed of light). By FFT of the temporal traces, as shown in Fig. 8(b), spectral interference fringes due to the etalon effect provide also an additional calibration of the THz frequency axis. Figures 8(c) and (d), respectively, report the retrieved refractive index and absorption coefficient of the GaAs sample in the frequency range from 0.3 to 2 THz. The results obtained by the OSCAT and DTM methods agree quite well within the experimental uncertainty and are compatible with those reported in previous measurements [33,34].

Optics EXPRESS

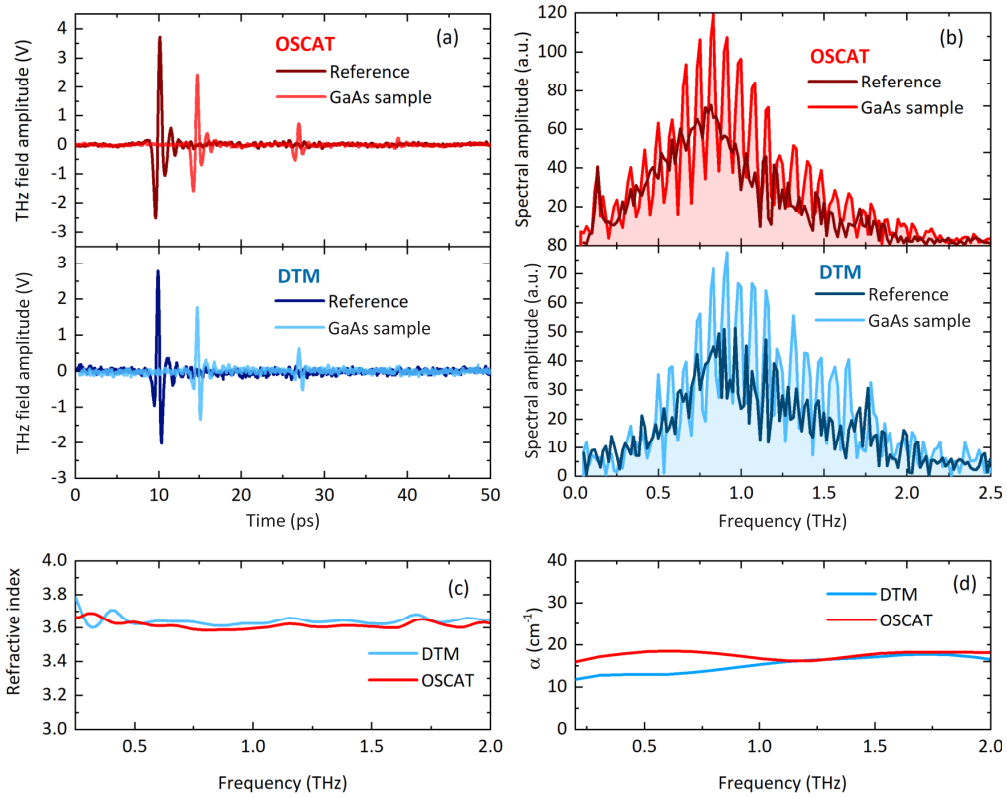

Fig. 8. (a) OSCAT (red curve) and DTM (light blue curve) signals transmitted by the 520-μm thick GaAs plate (dark red and blue curves represent the reference signal without the GaAs plate). (b) Spectra corresponding to the time trace reported in (a). Retrieved (c) refractive index and (d) absorption coefficient of the GaAs sample.

4. Conclusion

The comprehensive characterization of a compact THz-TDS instrument is presented based on a low-energy ultrafast Yb laser, with tunable pulse repetition frequency, and PCAs. The instrument can be operated in three different time-domain configurations, allowing a versatile use for a wide range of applications depending on the different measurement requirements: high-sensitivity, fast acquisition, phase-sensitive sensing. Further improvement of the spectrometer performance can be obtained, in terms of THz bandwidth and efficiency, by using enhanced PCAs optimized for 1 μm pump wavelength, and in terms of fast acquisition times, by adopting intracavity electrooptic modulator and longer optical fiber delay line.

Acknowledgments. L. M. Molteni thanks the Italian National Research Council (CNR) and Confindustria for the PhD scholarship.

Disclosures. The authors declare no conflicts of interest.

Data availability. Data underlying the results presented in this paper are not publicly available at this time but may be obtained from the authors upon reasonable request.

References

1. I. Amenabar, F. Lopez, and A. Mendikute, "In introductory review to THz non-destructive testing of composite mater," J. Infrared, Millimeter, Terahertz Waves **34**(2), 152–169 (2013).
2. S. Zhong, "Progress in terahertz nondestructive testing: A review," Front. Mech. Eng. **14**(3), 273–281 (2019).

Optics EXPRESS

3. K. Kawase, Y. Ogawa, Y. Watanabe, and H. Inoue, "Non-destructive terahertz imaging of illicit drugs using spectral fingerprints," Opt. Express **11**(20), 2549–2554 (2003).
4. J. P. Guillet, B. Recur, L. Frederique, B. Bousquet, L. Canioni, I. Manek-Hönninge, P. Desbarats, and P. Mounaix, "Review of terahertz tomography techniques," J. Infrared, Millimeter, Terahertz Waves **35**(4), 382–411 (2014).
5. L. A. Sterczewski, J. Westberg, Y. Yang, D. Burghoff, J. Reno, Q. Hu, and G. Wysocki, "Terahertz hyperspectral imaging with dual chip-scale combs," Optica **6**(6), 766–771 (2019).
6. N. A. Aghamiri, F. Huth, A. J. Huber, A. Fali, R. Hillenbrand, and Y. Abate, "Hyperspectral time-domain terahertz nano-imaging," Opt. Express **27**(17), 24231–24242 (2019).
7. J. Zhao, E. Yiwen, K. Williams, X.-C. Zhang, and R. W. Boyd, "Spatial sampling of terahertz fields with sub-wavelength accuracy via probe-beam encoding," Light: Sci. Appl. **8**(1), 55 (2019).
8. L. Olivieri, J. S. Totero Gongora, L. Peters, V. Cecconi, A. Cutrona, J. Tunesi, R. Tucker, A. Pasquazi, and M. Peccianti, "Hyperspectral terahertz microscopy via nonlinear ghost imaging," Optica **7**(2), 186–191 (2020).
9. H. B. Liu, H. Zhong, N. Karpowicz, Y. Chen, and X. C. Zhang, "Terahertz spectroscopy and imaging for defense and security applications," Proc. IEEE **95**(8), 1514–1527 (2007).
10. A. G. Davies, A. D. Burnett, W. Fan, E. H. Linfield, and J. E. Cunningham, "Terahertz spectroscopy of explosives and drugs," Mater. Today **11**(3), 18–26 (2008).
11. M. Hangyo, M. Tani, and T. Nagashima, "Terahertz time-domain spectroscopy of solids: a review," Int. J. Infrared Millimeter Waves **26**(12), 1661–1690 (2005).
12. M. Naftaly and R. E. Miles, "Terahertz time-domain spectroscopy for material characterization," Proc. IEEE **95**(8), 1658–1665 (2007).
13. C. Yu, S. Fan, Y. Sun, and E. Pickwell-MacPherson, "The potential of terahertz imaging for cancer diagnosis: a review of investigations to date," Quant. Imag. Med. Surg. **2**(1), 33–45 (2012).
14. S. Zong, G. Ren, S. Li, B. Zhang, J. Zhang, W. Qi, J. Han, and H. Zhao, "Terahertz time-domain spectroscopy of L-histidine hydrochloride monohydrate," J. Mol. Struct. **1157**, 486–491 (2018).
15. Y. Ueno and K. Ajito, "Analytical terahertz spectroscopy," Analyt. Sci. **24**(2), 185–192 (2008).
16. H. W. Hübers, M. F. Kimmitt, N. Hiromoto, and E. Bründermann, "Terahertz Spectroscopy: System and Sensitivity Considerations," IEEE Trans. THz Sci. Technol. **1**(1), 321–331 (2011).
17. E. B. Moon, T. I. Jeon, and D. R. Grischkowsky, "Long-path THz-TDS atmospheric measurements between buildings," IEEE Trans. Terahertz Sci. Technol. **5**(5), 742–750 (2015).
18. H. Elayan, O. Amin, B. Shihada, R. M. Shubair, and M.-S. Alouini, "Terahertz band: The last piece of RF spectrum puzzle for communication systems," IEEE Open J. Commun. Soc. **1**, 1–32 (2020).
19. W. Withayachumnankul and M. Naftaly, "Fundamentals of Measurement in Terahertz Time-Domain Spectroscopy," J. Infrared Milli. Terahz. Waves **35**(8), 610–637 (2014).
20. J. Neu and C. A. Schmuttenmaer, "Tutorial: An introduction to terahertz time domain spectroscopy (THz-TDS)," J. Appl. Phys. **124**(23), 231101 (2018).
21. J. Xu and X. C. Zhang, "Circular involute stage," Opt. Lett. **29**(17), 2082–2084 (2004).
22. H. Kitahara, M. Tani, and M. Hangyo, "High-repetition-rate optical delay line using a micromirror array and galvanometer mirror for a terahertz system," Rev. Sci. Instrum. **80**(7), 076104 (2009).
23. T. Yasui, E. Saneyoshi, and T. Araki, "Asynchronous optical sampling terahertz time-domain spectroscopy for ultrahigh spectral resolution and rapid data acquisition," Appl. Phys. Lett. **87**(6), 061101 (2005).
24. T. Yasui, Y. Kabetani, E. Saneyoshi, S. Yokoyama, and T. Araki, "Terahertz frequency comb by multifrequency-heterodyning photoconductive detection for high-accuracy, high-resolution terahertz spectroscopy," Appl. Phys. Lett. **88**(24), 241104 (2006).
25. R. J. B. Dietz, N. Vieweg, T. Puppe, A. Zach, B. Globisch, T. Göbel, P. Leisching, and M. Schell, "All fiber-coupled THz-TDS system with kHz measurement rate based on electronically controlled optical sampling," Opt. Lett. **39**(22), 6482–6485 (2014).
26. R. Wilk, T. Hochrein, M. Koch, M. Mei, and R. Holzwarth, "OSCAT: Novel Technique for Time-Resolved Experiments Without Movable Optical Delay Lines," J. Infrared Milli. Terahz Waves **32**(5), 596–602 (2011).
27. T. Furuya, E. S. Estacio, K. Horita, C. T. Que, K. Yamamoto, F. Miyamaru, S. Nishizawa, and M. Tani, "Fast-Scan Terahertz Time Domain Spectrometer Based on Laser Repetition Frequency Modulation," Jpn. J. Appl. Phys. **52**(2R), 022401 (2013).
28. N. M. Burford and M. O. El-Shenawee, "Review of terahertz photoconductive antenna technology," Opt. Eng. **56**(1), 010901 (2017).
29. R. Wilk, T. Hochrein, M. Koch, M. Mei, and R. Holzwarth, "Terahertz spectrometer operation by laser repetition frequency tuning," J. Opt. Soc. Am. B **28**(4), 592–595 (2011).
30. F. Amirkhan, M. Gratuze, X. Ropagnol, T. Ozaki, F. Nabki, and F. Blanchard, "Terahertz time-domain derivative spectrometer using a large-aperture piezoelectric micromachined device," Opt. Express **29**(14), 22096–22107 (2021).
31. L. M. Molteni, F. Canella, F. Pirzio, M. Betz, E. Vicentini, N. Coluccelli, G. Piccinno, A. Agnesi, P. Laporta, and G. Galzerano, "Low-noise Yb:CALGO Optical Frequency Comb," Opt. Express **29**(13), 19495–19505 (2021).
32. I. E. Gordon, L. S. Rothman, and R. J. Hargreaves et al., "The HITRAN2020 molecular spectroscopic database," J. Quant. Spectrosc. Radiat. Transf. **277**, 107949 (2022).
33. T. D. Dorney, R. G. Baraniuk, and D. M. Mittleman, "Material parameter estimation with terahertz time-domain spectroscopy," J. Opt. Soc. Am. A **18**(7), 1562–1571 (2001).
34. E. Mavrona, F. Appugliese, J. Andberger, J. Keller, M. Franckié, G. Scalari, and J. Faist, "Terahertz refractive index matching solution," Opt. Express **27**(10), 14536–14544 (2019).